Chinese Chemical Letters 35 (2024) 109803

Contents lists available at ScienceDirect

Chinese Chemical Letters

journal homepage: www.elsevier.com/locate/cclet

"Co-coordination force" assisted rigid-flexible coupling crystalline polymer for high-performance aqueous zinc-organic batteries

Jun Guo [a,b], Zhenbang Zhuang [b,c], Wanqiang Liu [a,*], Gang Huang [b,*]

[a] School of Materials Science and Engineering, Changchun University of Science and Technology, Changchun 130022, China
[b] State Key Laboratory of Rare Earth Resource Utilization, Changchun Institute of Applied Chemistry, Chinese Academy of Sciences, Changchun 130022, China
[c] Key Laboratory of Automobile Materials, Ministry of Education, Department of Materials Science and Engineering, Jilin University, Changchun 130022, China

ARTICLE INFO

Article history:
Received 18 February 2024
Revised 8 March 2024
Accepted 20 March 2024
Available online 21 March 2024

Keywords:
Co-coordination force
Crystalline polymer
Hydrogen bonds
Organic electrode materials
Aqueous zinc-ion batteries

ABSTRACT

Organic electrode materials (OEMs) have attracted substantial attention for aqueous zinc-ion batteries (AZIBs) due to their advantages in relieving resource and environmental anxiety. However, the potential of OEMs is plagued by their low achievable capacity and high solubility. Here, we have proposed a new concept of "co-coordination force" and designed a rigid-flexible coupling crystalline polymer that can overcome the abovementioned limitations. The obtained crystalline polymer (BQSPNs) with multiredox centres makes the BQSPNs exist intermolecular hydrogen bonds (HB) among -C=O, -C=N, and -NH and consequently exhibits transverse two-dimensional arrays and longitudinal π-π stacking structure. Additionally, *in-situ* FTIR, Raman, variable temperature FTIR spectra, and 2D nuclear overhauser effect spectroscopy (NOESY) well capture the existence and evolution process of HB during the electrochemistry reaction process of BQSPNs, uncovering the effect of HB in stabilizing the structure and promoting the reaction kinetics. As a result, the BQSPNs with rationally designed "co-coordination force" deliver a high capacity of 459.6 mAh/g and a stable cycling lifetime for more than 100,000 cycles at 10 A/g in AZIBs. Our results disclose the HB effect and provide a brand-new strategy for high-performance OEMs design.

The pursuit of large-scale electrochemical energy storage systems, particularly those focused on green energy, remains a subject of considerable attention [1]. This stems from the growing concerns about resource availability triggered by the escalating energy management requirements in our daily lives [2]. Presently, substantial efforts are directed towards advancing the development of battery systems that are greener, safer, and more sustainable [3]. Among them, aqueous zinc-ion batteries (AZIBs) exhibit significant promise for next-generation energy storage, particularly within large-scale energy storage systems [4]. This is attributed to their myriad advantages over existing electrochemical systems, encompassing cost-effectiveness, heightened safety, and eco-friendliness [5,6]. Thus, the selection of cathode materials plays a pivotal role in the construction of durable AZIBs. Traditionally metal-based inorganic compounds, such as manganese, vanadium-based oxides, for AZIBs electrodes have been widely reported, which follow an intercalation/conversion mechanism during the charge/discharge process [7,8]. Nevertheless, the large crystal lattice evolution, significant volume structural strain, and irreversible dissolution during the frequent insertion process of Zn^{2+} will lead to low cyclability [9]. In addition, the use of toxic or polluting elements, non-renewable resources, and unsustainable synthetic paths within these kinds of electrode materials also run counter to the design criteria of green and sustainable chemistry energy [10]. To this end, organic electrode materials (OEMs), especially polymer materials, have been widely investigated in AZIBs for their stable, cost-effective, and sustainable features [11,12]. Regrettably, traditional polymers tend to pack efficiently in a dense amorphous solid state, displaying minimal or absent crystallinity and regular morphology [13,14]. These characteristics would inevitably give rise to drawbacks including sluggish energy conversion efficiency, limited adjustability, and challenges in comprehending the intricacies of the electrochemical reaction mechanism [15]. In particular, the consideration of environmental friendliness and sustainable synthetic pathways have been frequently overlooked during the OEMs design, which is a huge obstacle in the large-scale application of OEMs. Therefore, proposing and exploring innovative concepts to design new polymer materials possessing stable struc-

* Corresponding authors.
E-mail addresses: wqliu1979@126.com (W. Liu), ghuang@ciac.ac.cn (G. Huang).

https://doi.org/10.1016/j.cclet.2024.109803
1001-8417/

tures and sustainable synthesis routes is urgent and significant for practical applications. Inspired by this, organic crystalline polymers (OCPs) made of aromatic polymer chains bonding with van der Waals forces, π-π stacking interaction or hydrogen bonds (HB) are readily form various channels and voids amongst the molecules and have excellent deformation ability [15]. Compared to the amorphous polymers, the OCPs with clear crystalline structures provide energetically advantageous ion migration pathways, effectively avoiding the loss of active sites and the decrease of coulombic efficiency caused by ion disturbance to polymer chains. When compared to the inorganic crystal materials, the OCPs featuring large conjugated systems typically exhibit high structural flexibility and reduced ion diffusion repulsion. These attributes could efficiently counteract the strong electrostatic interactions between the high-charge ions and the host lattice, preventing the structural collapse induced by the phase transformations during ion intercalation/extraction processes. Moreover, OCPs, primarily composed of elements such as C, N, and O, boast environmental friendliness and biodegradability. Meanwhile, the abundant carbonyl or amino groups within the conjugated structures could enhance their chemical reactivity towards Zn^{2+}. These distinctive characteristics make the OCPs act as highly promising OEMs for advanced AZIBs.

Herein, we have introduced a new concept of "co-coordination force" and exemplified it through the design of rigid-flexible coupling crystalline polymers, denoted as BQSPNs. These polymers serve as a proof-of-concept demonstration within OEMs benefiting from their abundant electroactive sites (*e.g.*, C=O and C=N groups) and stable interchain structures. Employing rational molecular engineering, the rigid conjugated moieties of BQSPNs are linked with flexible reactive groups to assemble polymer arrays. These arrays are subsequently packed *via* intermolecular π–π stacking and HB interactions, resulting in the formation of crystalline domains. Ultimately, the rigid-flexible coupling BQSPNs are characterized with a π-π stacking structure and HB networks formed by the electronic delocalization polarize among C=O, N-H, and C=N groups. Moreover, the existence and evolution process of HB during the electrochemistry reaction of BQSPNs has been well studied, disclosing the effect of HB in stabilizing the structure and promoting the reaction kinetics of BQSPNs. As a result, the BQSPNs achieve a high capacity of 459.6 mAh/g, an outstanding cycle life of over 100,000 cycles with 68% retention at 10 A/g. This study introduces an innovative structure design concept aimed at enhancing the electrochemical performance of OEMs and elucidating the HB evolution during the electrochemical reaction process.

Although benzoquinone (BQ) stands as a fundamental energy storage unit with high theoretical capacity (496 mAh/g) and a rigid structure, its practical electrochemical performance within AZIBs falls short of the desired ideal (Fig. S1 in Supporting information). Nonetheless, it is important to acknowledge that the utilization of fundamental energy storage units with notable theoretical capacity remains integral to the prospective design of OEMs. Consequently, we will focus on investigating the pivotal question that how the active site environment influences its energy storage capabilities. To answer this question, a series of compounds featuring identical active sites in terms of type, number, and position, but varying in chemical environments was strategically designed to establish the correlation between the properties of active sites environment and its influence on battery performance. In the initial phase, two distinct types of groups were employed to influence the chemical environment surrounding the C=O groups within the benzoquinone skeleton. Remarkably, the incorporation of either electron-withdrawing groups or electron-pushing groups facilitates the coordination process between the carbonyl group and Zn^{2+} (Fig. S2 in Supporting information).

This outcome contrasts with prior findings, where enhanced electrochemical performance was attributed to the introduction

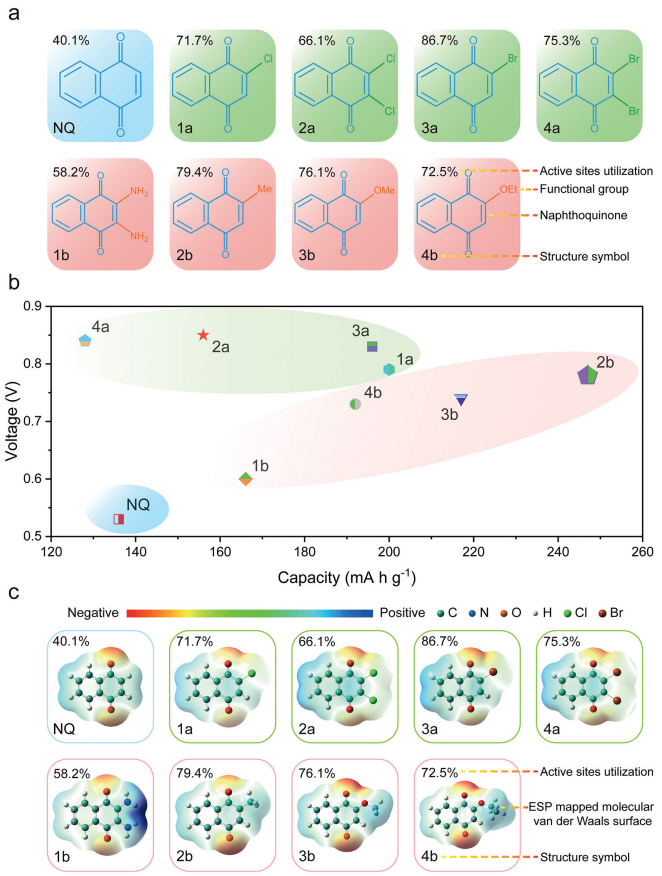

Fig. 1. (a) Library of the NQ and NQ derivatives. (b) Voltages and capacities of the NQ derivative-based cathodes. (c) The ESP mapped molecular van der Waals surface of the NQ derivatives.

of electron-withdrawing groups [16,17]. Intriguingly, we have observed that the introduction of both groups coincides with the emergence of weak interactions, including HB or halogen bond (XB), within the system [18,19]. Simultaneously, these weak interactions, such as HB or XB, are regarded as assisting forces that predominantly contribute to the coordination process. Consequently, we propose that this form of auxiliary coordination force may be appropriately termed a "co-coordination force" within the context of AZIBs. With such a point, the expanded organic skeleton (Naphthoquinone, NQ) has been chosen as the fundamental unit featuring two distinct groups (electron-withdrawing/pushing groups) (Fig. 1a). This choice is aimed at establishing the universality of the "co-coordination force" principle within AZIBs. As a result, a range of NQ derivatives has been successfully synthesized and evaluated as cathode materials for AZIBs, including four electron-withdrawing group derivatives (1a, 2a, 3a, and 4a), as well as four electron-pushing group derivatives (1b, 2b, 3b, and 4b). A concise table provides a comprehensive overview of NQ derivatives, distinguished by electron-withdrawing (green) and electron-pushing (pink) groups, in order to substantiate our argument regarding the "co-coordination force" (Fig. 1a). Detailed synthesis recipes, reaction conditions, and characterization are listed in the supporting information. Evidently, incorporating either electron-withdrawing and electron-pushing groups lead to a substantial enhancement in utilization of the active sites on NQ derivatives (Fig. 1b and Fig. S3 in Supporting information). The active site utilization means the ratio of the actual specific capacity to the theoretical specific capacity. To further validate these findings, density functional theory (DFT) calculations were carried out (Fig. 1c). Potential active sites were deduced through the method of electrostatic potential

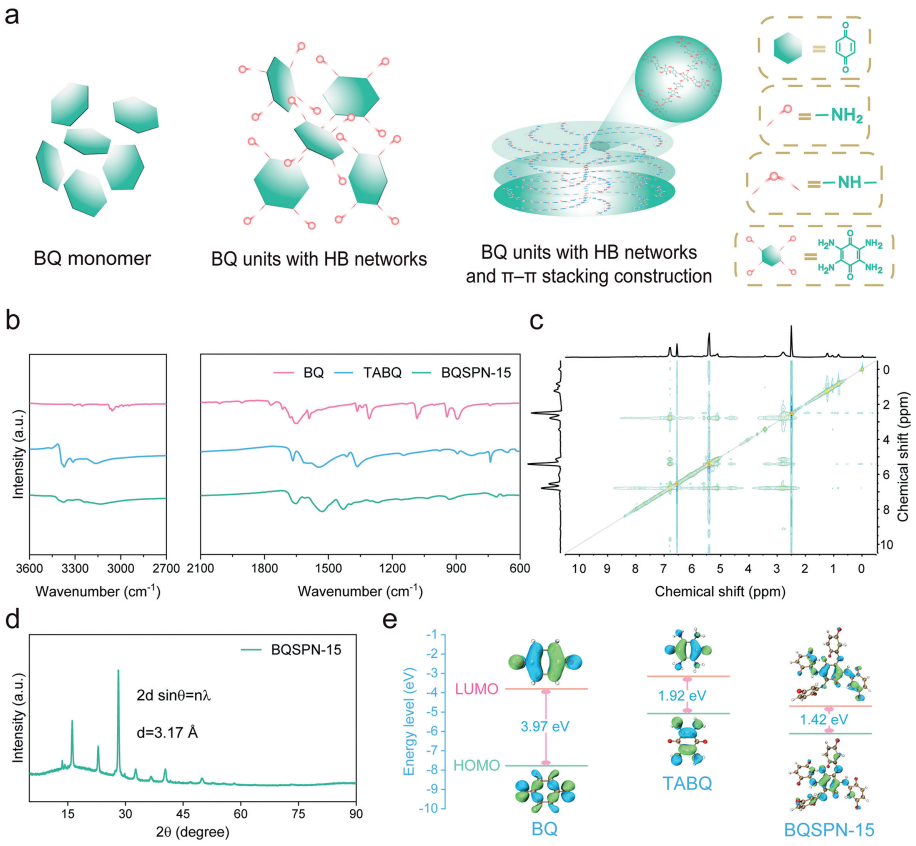

Fig. 2. (a) Schematic illustration for the design route through the method of introducing HB networks. (b) FTIR spectra of the BQ, TABQ, and BQSPN-15. (c) 2D ^{1}H-^{1}H NOESY and (d) XRD spectra of the BQSPN-15. (e) HOMO/LUMO energy levels and orbit distribution of the BQ, TABQ, and BQSPN-15.

(ESP) from the perspective of electrophilic or nucleophilic reaction, since the insertion of cation is an electrophilic reaction process that most probably occur at around the negative ESP value reactive sites (carbonyl group) [1]. It is noteworthy that no additional active sites have been introduced by during process. Therefore, the sole shared factor is the emergence of fresh weak interactions (HB or XB) around active sites, facilitating coordination with Zn^{2+}. This outcome provides additional validation for the "co-coordination force" hypothesis. Drawing inspiration from this concept, we employ the basic rigid conjugated moieties (BQ) as building blocks, establishing a sturdy polymer structure. These building blocks interconnect with high theoretical capacity "co-coordination force" based flexible groups (N–H) [20,21], resulting in the creation of the rigid–flexible coupling crystalline polymers. Simultaneously, the incorporation of N–H could be partly oxidized to the active sites (C=N), forms the HB interactions to enhance the active site's coordination capability towards Zn^{2+} and reinforces the structural stability, contributing to a comprehensively enhance in electrochemical performance.

Fig. 2a illustrates the design process of BQSPNs, depicting its structural evolution. As the continuously rising of HB numbers and molecular weight of the structure, from BQ to TABQ, and finally to BQSPNs, the overall stability of the structure also undergoes a corresponding enhancement. In addition, it is important to highlight that the molecular weight and other microstructural aspects of the final BQSPNs can be readily adjusted by altering the reactant ratios. The resulting BQSPNs are denoted as BQSPN-n, where n represents the molar ratio of reactants. Consequently, BQSPN-15 has been selected for the following part of structure characterization and electrochemical performance testing, and the specific justifications for this choice was elaborated upon in the supporting information part. When the primary ammonia was first introduced into BQ skeleton to obtain TABQ, the active sites utilization and thermodynamic stability increase simultaneously due to the establishment of HB networks. Different from the room-temperature sublimation of BQ under vacuum, the sublimation temperature of TABQ is much higher and can only start from 200 °C, revealing that the formation of HB networks among TABQ could significantly increase its stability (Figs. S4 and S5 in Supporting information). This can be further confirmed by the thermogravimetric analysis (TGA), where the TABQ shows a higher high-temperature resistance than BQ (Fig. S6 in Supporting information). As can be seen from the FTIR spectra in Fig. 2b, the -NH_2 renders the C=O stretching vibration redshift from 1770 cm^{-1} to 1667 cm^{-1}, indicating the formation of HB networks. Compared with TABQ, the BQSPN-15 has a better thermodynamic stability (Figs. S4-S6), and the carbonyl peak further redshifts to 1651 cm^{-1}, which due to the higher molecular weight, more HB networks and π-π stacking interactions. The HB networks can be supported by the ^{1}H-^{1}H NOESY analysis. As shown in Fig. 2c, the NOE cross peak between the amino chemical shifts can be clearly observed for BQSPN-15, indicating the existence of HB [22]. Aside from the FTIR and ^{1}H-^{1}H NOESY measurements, the X-ray diffraction (XRD) pattern was also recorded to demonstrate the crystal structure of BQSPN-15. Fig. 2d illustrates that the BQSPN-15 represents more pronounced peaks compared to the majority of polymer electrodes for organic batteries. Specifically, the discernible peak at 28.1° indicates a clear π-π stacking diffraction ($d = 3.17$ Å) [23–25]. These findings collectively support the formation mechanism of BQSPNs, where the rigid BQ units are interconnected with flexible reactive groups, resulting in the formation of polymer arrays. Subsequently, these arrays pack together through intermolecular π–π stacking and HB interactions, forming

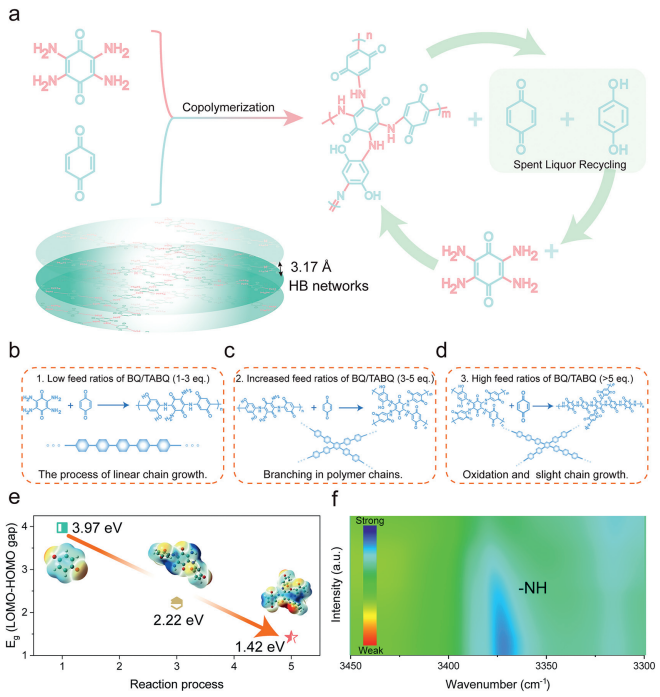

Fig. 3. (a) Schematic illustration for the synthesis of BQSPNs. Possible reaction process at (b) low (1–3 equiv.), (c) medium (3–5 equiv.), and (d) high (>5 equiv.) feed ratios of BQ/TABQ. (e) The E_g (LUMO-HOMO gap) during the polymerization process. (f) *In-situ* variable temperature FTIR spectra of the BQSPN-15.

crystalline domains. In addition, the rationality of our design is further substantiated by DFT calculations. Introducing co-coordination force based -N-H groups to link rigid conjugated BQ units obtain the narrowest E_g (LOMO–HOMO, 1.42 eV) compared to both BQ (3.97 eV) and TABQ (1.92 eV), as shown in Fig. 2e. Thus, BQSPNs possess exceptional intrinsic conductivity due to the positive relationship between electronic conductivity and E_g, resulting in superior rate performance in AZIBs and validating our design strategy [26].

Besides the rationality of macro structure, the environmental friendliness of synthetic process and the controllability of microconfigurations are crucial factors for the practical application of OEMs in large-scale energy storage systems. As depicted in Fig. 3a, the BQSPNs have been synthesized *via* a one-step process utilizing BQ and TABQ as precursors under mild reaction conditions and green solvents, rendering the entire synthesis environmentally sustainable and waste-free. The detailed experimental process is outlined in Fig. S7 (Supporting information), which is particularly advantageous for producing electrode materials on a large scale for energy storage systems. This advantage stems from its high recycling yield, continuous reactions, and waste-free synthesis process. Moreover, the reaction mechanism is also explored that BQ monomer plays the part of the dual role (reactant and oxidant) during the process of polymerization (Figs. S8-S10 in Supporting information), which can not only eliminate the need for expensive metal or non-metal catalysts in the polymerization reaction, reducing the overall reaction cost, but also circumvents the need for removing impurities (Fig. S11 in Supporting information). The polymer precipitates directly from the solution system. Consequently, the unprocessed filtrate consists solely of excess benzoquinone and phenol. Importantly, this method enables continuous electrode material production by simply replenishing the monomer solution into the reaction system, achieving a "zero discharge" of waste liquid. Further, the possible reaction process has been explored by NMR spectra (Figs. S9-S11), gel permeation chromatography (GPC) (Fig. S12 in Supporting information), and dynamic light scattering (DLS) (Fig. S14 in Supporting information). The formation of the polymer involves a sequential process of linear growth (Fig. 3b), branching (Fig. 3c), and oxidation accompanied by slight chain growth (Fig. 3d), as the BQ/TABQ feed ratios increase. Additionally, DFT calculations were conducted to study the rection process. As depicted in Fig. 3e, the polymerization process, from monomer (3.97 eV) through linear chain growth (2.22 eV) to branching (1.42 eV), exhibits a decreasing trend in E_g, ensuring the favorable rate performance of BQSPNs. Based on the aforementioned results and analysis, it is evident that BQSPNs featuring with a green synthetic process and controllable microconfiguration, including molecular weight, functional group ratio, and size. Given the potential existence of enrich HB types in BQSPN-15, such as N-H···O, N-H···N, N-H···N-H, C=O···H, and C=N···H, the FTIR spectra was used to confirm the types of HB in the following parts.

As illustrated in Fig. S15a (Supporting information), BQSPN-15 has four peaks at the range of 3480–2800 cm^{-1}, the peak at 3374 cm^{-1} belongs to the bending vibration of free N-H. In addition, three associated peaks of N-H at 3320 ($V_{N\text{-}H\cdots O}$), 3236 ($V_{N\text{-}H\cdots N}$), and 3130 cm^{-1} ($V_{N\text{-}H\cdots N\text{-}H}$) are detected. Notably, the wavenumber gap between free N-H peak and associated N-H···X peak due to the formation of HB. Furthermore, during the rage of 1750–1300 cm^{-1}, the peaks at 1651, 1610, 1528, 1489, 1429, and 1394 cm^{-1} are respectively belonging to the vibration of C=O, C=O···H, C=N, N-H, $Ar_{C=C}$, and C=N···H (Fig. S15b in Supporting information) [25]. To further clarify the existence of HB interactions in BQSPN-15, the *in-situ* variable temperature FTIR is applied to the study of the change of structure with temperature. Generally, the H-bond interaction would be gradually weakened as the rising of temperature and then resulting in a peak shift in the FTIR spectra [27]. As depicted in Fig. 3f, the N-H stretching vibration peak blueshift from 3374 cm^{-1} to 3381 cm^{-1} and its associated peaks gradually decrease in intensity with the temperature increases from r.t. to 180 °C, proving the existence of HB interactions [28]. Thus, the above characterization results have confirmed the existence and types of HB in BQSPN-15 and proved the effect on enhancing stability and electrochemical performance.

To disclose the HB effect and structure evolution of BQSPN-15 during the process of charging and discharging, the *in-situ* FTIR is used to probe the evolution of crystalline polymer structure. Before this process, the FTIR spectra of electrolyte, binder, BQSPN-15, and conductive additive are first tested to eliminate interference peaks, and the detailed discussion is list in Fig. S15 (Supporting information). Then, the FTIR spectra evolution of major groups (-NH, C=O, and C=N) on BQSPN-15 during the process of charging and discharging are shown in Fig. 4. The titanium mesh is used to load BQSPN-15 cathode that the IR light can pass through the cathode and obtain the *in-situ* FTIR spectroscopy (Fig. 4a). Comprehensively, the stretching vibration and bending vibration of N-H and its associated peaks spectra area located at 3100–3380 and 1450–1550 cm^{-1}. The stretching vibration of C=O and its associated peaks located at 1640–1670 cm^{-1}, and that of C=N at 1375–1520 cm^{-1} (Fig. 4b).

During the discharging process, the peak of the active site C=N at around 1560 cm^{-1} and its associated peaks N-H···N and C=N···H at around 3245 and 1394 cm^{-1} weaken continuously (Fig. 4c) accompanied by the blueshift of N-H, indicating the transformation of C=N and C-N^- anions accompanied with the weaken of HB around N-H. Simultaneously, the peak corresponding to C=O vibration at 1667 cm^{-1} (Fig. 4d) and its associated peaks N-H···O and C=O···H at 3320 and 1646 cm^{-1} also experiences a continuous decrease in intensity, showing the transformation of C=O to C-O^-. For the charging process, whether the peak intensity of active sites (C=O and C=N) or their associated peaks exhibits a reverse trend,

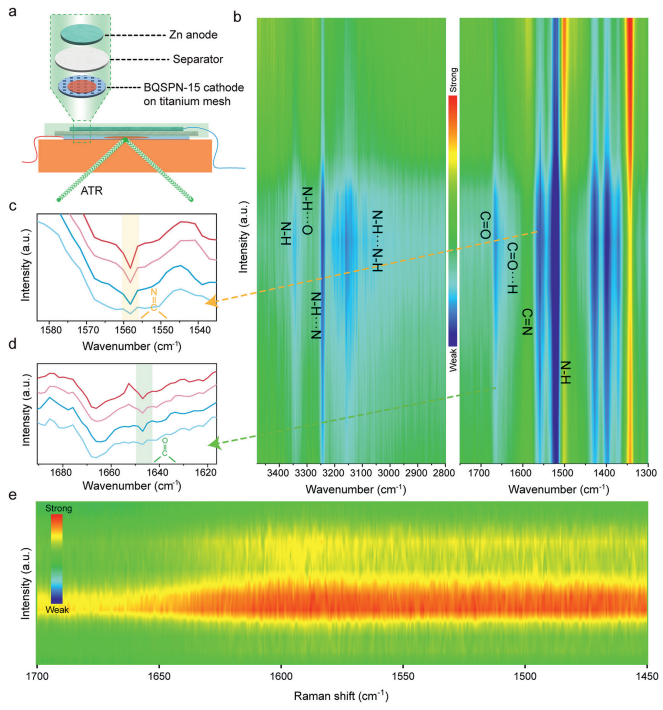

Fig. 4. (a) Schematic diagram of *in-situ* FTIR analysis. (b) *In-situ* FTIR spectra of the BQSPN-15 cathode during the electrochemistry process. Changes of (c) C=N and (d) C=O during the discharge process *in-situ* FTIR spectra. (e) *In-situ* Raman spectrum of the BQSPN-15 cathode during the electrochemistry process.

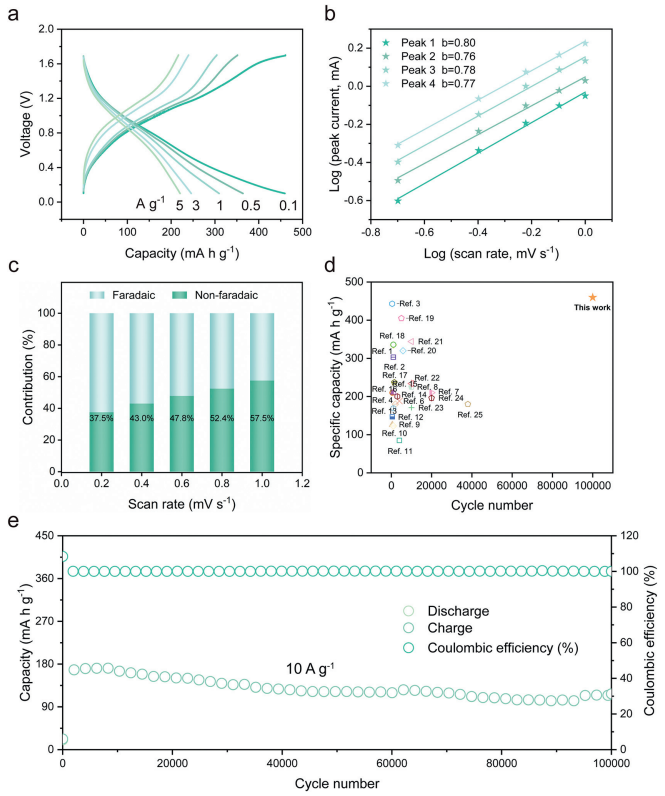

Fig. 5. (a) Discharge/charge curves of BQSPN-15//Zn batteries at different current densities. (b) Power law dependence of the measured current on scan rate at corresponding peak potentials. (c) Contribution ratios of the capacitive charge storage at different scan rates. (d) Capacity and cycle life comparison with the reported cathode materials in AZIBs (the numbers refer to references in Supporting Information). (e) Cycling performance of the BQSPN-15 at 10 A/g.

manifesting the better reversibility of active sites and HB interactions [29]. This reversible change of C=O and C=N during cycling is also verified by *in-situ* Raman spectrum, in which the results are well in accordance with that of the *in-situ* FTIR spectra (Fig. 4e). Then, X-ray photoelectron spectroscopy (XPS) of the BQSPN-15 electrodes at different stages were acquired to further elucidate its evolution of groups, which clearly certifies the better reversibility of active sites during the discharge and charge processes (Fig. S16a in Supporting information). As shown in Fig. S16b (Supporting information), the O 1s XPS spectra provide powerful evidence for the reversible transformation between C=O and C-O$^-$ during a single cycle process. Meanwhile, the N 1s signal of C=N weakens in intensity as the discharge process goes on (from a to d) and then gradually returned during charging process (from d to h) (Fig. S16c in Supporting information). This variation tendency of C=O and C=N are in accordance with the *in-situ* FTIR/Raman analysis and corroborates the better reversible reaction of C=O and C=N groups.

For OEMs, a highly reversibility of active sites means a better cycling performance and capacity stability [30]. In addition, for the whole electrochemical system, the ion storage mechanism is equally important. Given the potential existence of multiple charge storage mechanisms in OEMs encountered in AZIBs [31], such as the individual storage of Zn^{2+} or H^+, or co-storage of Zn^{2+} and H^+, a series of *ex-situ* characterizations were carried out to thoroughly investigate its structure and composition evolution during the charge and discharge processes in the following parts. As demonstrated in Fig. S17a (Supporting information), the Zn 2p XPS spectra provide powerful evidence for certifying the storage and release of Zn^{2+} in the BQSPN-15 during the discharge and charge processes. In addition, the emergence of the S 2p peak can be ascribed to the H^+ consumption induced formation of $Zn_4(OH)_6SO_4{\cdot}5H_2O$ (Fig. S17b in Supporting information). Generally, OH^- would continuously generate through the consumption of H^+ in BQSPN-15 during the discharge process in $ZnSO_4$ electrolyte. The formed OH^- can react with $ZnSO_4$ to form $Zn_4(OH)_6SO_4{\cdot}5H_2O$ [32]. Such process is evidenced by the XRD patterns. Fig. S18 (Supporting information) shows that the diffraction peaks of $Zn_4(OH)_6SO_4{\cdot}5H_2O$ appear in the discharged state and disappear after the following charge process, which is consistent with the results of XPS [20]. Aside from the XPS and XRD measurements, the *ex-situ* FTIR spectra were also recorded to validate the H^+ storage process. Compared with *in-situ* FTIR spectra, the use of *ex-situ* FTIR can eliminate the interference of H_2O on hydroxyl characteristic peak in aqueous electrolyte. As depicted in Fig. S19 (Supporting information), the appearance of a characteristic peak from the stretching vibration of -OH at around 3240 cm^{-1} during the discharge process and its disappearance in the subsequent recharge process reveals the stored cations containing H^+ and its high reversibility in BQSPN-15 [33]. To sum up, the above results strongly support the occurrence of Zn^{2+}, H^+ co-(de)storage behavior in BQSPN-15 during the charge/discharge process.

Further, the kinetic performance and cycling stability of the BQSPN-15 are studied to confirm the HB effect in BQSPN-15//Zn batteries. As shown in Fig. 5a, the BQSPN-15 shows stable reversible capacities of 459.6, 363.9, 309.3, 245.8, and 220.3 mAh/g at current densities of 0.1, 0.5, 1.0, 3.0, and 5.0 A/g, respectively. Compared to BQ monomer, BQSPN-15 displays the absolute advantages in terms of capacity, electrolyte wettability, and charge transfer impedance (Figs. S20 and S21 in Supporting information). Moreover, when decreasing the current density from 5 A/g to 0.1 A/g, the capacity shows a notable ability to restore to the initial value, demonstrating the considerable rate capability and structural stability of the BQSPN-15 (Fig. S22 in Supporting information). Additionally, the redox kinetics of BQSPN-15 are elucidated

by the CV tests at different scan rates. As illustrated in Fig. S23 (Supporting information), there are no obvious changes in curve shape and polarization with the well-maintained redox peaks as the scan rate increases from 0.2 mV/s to 1.0 mV/s, indicating the better stability and reaction kinetics. Further, the corresponding *b* values (0.76–0.80) are calculated through the logarithmic relationship of peak current and scan rate (Fig. 5b). These high *b* values mean that the non-faradaic behaviors dominate the discharge/charge process, leading to a better rate capability [34–36]. As the scan rate rises from 0.2 mV/s to 1.0 mV/s, the ratio of charge storage contributed by non-faradaic process increases from 37.5% to 57.5% (Fig. 5c and Fig. S24 in Supporting information).

Accordingly, the BQSPN-15 achieves an outstanding cycle stability over 100,000 cycles with a high retention (68%) at 10 A/g (Fig. 5e). To the best of our knowledge, such a long cycling lifetime has surpassed most of the reported cathode materials in AZIBs (Fig. 5d) [37–43]. The above results demonstrate that the existence of HB effectively improves the utilization of active sites and the cycle stability of the polymer.

In summary, we have proposed a new concept of "co-coordination force" and designed a rigid-flexible coupling crystalline polymers (BQSPN-15) with π-π stacking and HB interactions by linking the rigid conjugated moieties (BQ) with the high-theoretical-capacity "co-coordination force" group (-NH-). The sustainable reaction path and synthesis process of BQSPN-15 with "zero discharge" of waste liquid are definitely more suitable for the construction of large-scale energy storage systems. In addition, the *in-situ* variable temperature FTIR spectra and NOESY spectroscopy confirm the existence of HB and the *in-situ* FTIR/Raman spectra witness the reversible evolution of HB and active sites during the electrochemical reaction process of BQSPN-15, demonstrating the HB can stabilize the structure and improve the achievable capacity. As a result, the BQSPN-15 delivers a high capacity of 459.6 mAh/g, a decent cycle life over 100,000 cycles with 68% retention at 10 A/g. Our work provides a new perspective on the influence of functional groups on the electrochemical properties of OEMs and details the significance of HB effect in organic batteries.

Declaration of competing interest

The authors declare that they have no known competing financial interests or personal relationships that could have appeared to influence the work reported in this paper.

Acknowledgments

This work was financially supported by the National Key R&D program of China (No. 2022YFB2402200), National Natural Science Foundation of China (Nos. 52271140, 52171194), Youth Innovation Promotion Association CAS (No. 2020230), Jilin Provincial Natural Fund (No. 20230101205JC), and National Natural Science Foundation of China Outstanding Youth Science Foundation of China (Overseas).

Supplementary materials

Supplementary material associated with this article can be found, in the online version, at doi:10.1016/j.cclet.2024.109803.

References

[1] Y. Lu, X.S. Hou, L.C. Miao, et al., Angew. Chem. Int. Ed. 58 (2019) 7020–7024.
[2] Q.J. Deng, Z.B. Luo, R. Yang, J.Z. Li, ACS Sustain. Chem. Eng. 8 (2020) 15445–15465.
[3] J. Geng, Y. Ni, Z. Zhu, et al., J. Am. Chem. Soc. 145 (2023) 1564–1571.
[4] Y.L. Liang, Y. Yao, Joule 2 (2018) 1690–1706.
[5] T. Janoschka, M.D. Hager, U.S. Schubert, Adv. Mater. 24 (2012) 6397–6409.
[6] C.P. Han, H.F. Li, R.Y. Shi, et al., J. Mater. Chem. A 7 (2019) 23378–23415.
[7] X.T. Zhang, J.X. Li, H.S. Ao, et al., Energy Storage Mater. 30 (2020) 337–345.
[8] C. Liu, W. Xu, C. Mei, et al., Adv. Energy Mater. 11 (2021) 2003902.
[9] F. Cheng, J. Liang, Z. Tao, J. Chen, Adv. Mater. 23 (2011) 1695–1715.
[10] T.P. Nguyen, A.D. Easley, N.A. Kang, et al., Nature 593 (2021) 61–66.
[11] F. Wan, L.L. Zhang, X.Y. Wang, et al., Adv. Funct. Mater. 28 (2018) 1804975.
[12] H.Y. Shi, Y.J. Ye, K. Liu, Y. Song, X. Sun, Angew. Chem. Int. Ed. 57 (2018) 16359–16363.
[13] M. Shaheen-Mualim, N. Kutner, S. Farah, Polym. Adv. Technol. 33 (2022) 3797–3799.
[14] X.Q. Tang, G.Y. Yan, J.W. Wang, et al., Polym. Adv. Technol. 33 (2022) 1628–1641.
[15] E. Lin, Z. Wang, X. Zhao, et al., Angew. Chem. Int. Ed. 61 (2022) e202117390.
[16] J. Kumankuma-Sarpong, S. Tang, W. Guo, Y. Fu, ACS Appl. Mater. Interfaces 13 (2021) 4084–4092.
[17] J.B. Wu, W. Xu, Y. Lin, et al., J. Power Sources 483 (2021) 229114.
[18] A. Mukherjee, G.R. Desiraju, Cryst. Growth Des. 11 (2011) 3735–3739.
[19] J. Matern, N. Baumer, G. Fernandez, J. Am. Chem. Soc. 143 (2021) 7164–7175.
[20] Y. Chen, J.Y. Li, Q. Zhu, et al., Angew. Chem. Int. Ed. 61 (2022) e202116289.
[21] Q. Zhang, Y. Ma, Y. Lu, et al., Nat. Commun. 11 (2020) 4463.
[22] M.R. Tuttle, S.T. Davis, S.Y. Zhang, ACS Energy Lett. 6 (2021) 643–649.
[23] S. Zheng, D. Shi, D. Yan, et al., Angew. Chem. Int. Ed. 61 (2022) e202117511.
[24] H. Gao, A.R. Neale, Q. Zhu, et al., J. Am. Chem. Soc. 144 (2022) 9434–9442.
[25] S.B. Zheng, D.J. Shi, T.J. Sun, et al., Angew. Chem. Int. Ed. 62 (2023) e202217710.
[26] L.W. Luo, W. Ma, P. Dong, et al., ACS Nano 16 (2022) 14590–14599.
[27] L. Jiao, Z.J. Du, X.M. Dai, et al., Polymer 247 (2022) 124792.
[28] L. Jiao, Y.N. Zhang, Z.J. Du, et al., J. Polym. Sci. 60 (2022) 2454–2464.
[29] N. Wang, Z.W. Guo, Z.G. Ni, et al., Angew. Chem. Int. Ed. 60 (2021) 20826–20832.
[30] T. Chen, H. Banda, L. Yang, et al., Joule 7 (2023) 986–1002.
[31] Y. Wang, C. Wang, Z. Ni, et al., Adv. Mater. 32 (2020) e2000338.
[32] Y.J. Gao, G.F. Li, F. Wang, et al., Energy Storage Mater. 40 (2021) 31–40.
[33] Z.R. Lin, H.Y. Shi, L. Lin, et al., Nat. Commun. 12 (2021) 4424.
[34] S. Li, J.D. Lin, Y.M. Zhang, et al., Adv. Energy Mater. 12 (2022) 2201347.
[35] Z. Xie, Z. Zhu, Z. Liu, et al., J. Am. Chem. Soc. 145 (2023) 25422–25430.
[36] Z. Liu, X. Zhang, J. Luo, Y. Yu, Chin. Chem. Lett. (2024), doi:10.1016/j.cclet.2024.109500.
[37] H. Xu, Y. Su, C. Zheng, et al., Chin. Chem. Lett. 35 (2024) 109173.
[38] Z. Zhu, T. Jiang, M. Ali, et al., Chem. Rev. 122 (2022) 16610–16751.
[39] M. Sun, Z. Wang, J. Jiang, X. Wang, C. Yu, Chin. Chem. Lett. 35 (2024) 109393.
[40] Y. Li, Y. Xu, X. Han, et al., Chin. Chem. Lett. 35 (2024) 109189.
[41] Y. Zhao, C. Yang, Y. Yu, Chin. Chem. Lett. 35 (2024) 108865.
[42] Y. Meng, M. Wang, J. Xu, et al., Angew. Chem. Int. Ed. 62 (2023) e202308454.
[43] X. Chen, H. Su, B. Yang, et al., Chin. Chem. Lett. 35 (2024) 108487.